

EUROPEAN COOPERATION
IN SCIENCE
AND TECHNOLOGY

CA20120 TD(22)01052
Bologna, Italy
Feb. 9th - 11th, 2022

EURO-COST

SOURCE: Brussels School of Engineering
Université libre de Bruxelles (ULB)

**Environment mapping with 28 GHz beamsteering transceivers: hardware architecture
and preliminary results**

Sami Chajii, Philippe De Doncker and François Quitin

50 Av. Roosevelt, 1050 Brussels, Belgium
Phone: +32-2-650-2829
Fax: –
Email: fquitin@ulb.be

Environment mapping with 28 GHz beamsteering transceivers: hardware architecture and preliminary results

Sami Chajji, Philippe De Doncker and François Quitin

Brussels School of Engineering, Université libre de Bruxelles (ULB)

Abstract—The evolution of radio communication systems towards millimeter-wave (mm-wave) frequencies allows for new opportunities in terms of localization and environment mapping. The increase in bandwidth and size of antenna arrays creates great similarities between 28 GHz communication systems and radar systems. There are several challenges to use 28 GHz communication systems for environment mapping: 1) it is unclear whether multipath components can be identified with arrays that rely on beamsteering, 2) the local oscillator (LO) is not shared between the transmitter and the receiver, causing considerable LO frequency offsets, and 3) the high power of the line-of-sight component tends to “blind” the receiver to all other multipath. In this paper, we realize (relatively) low-cost 28 GHz software-defined radio-based transceivers that use 4×4 antenna arrays. The transceiver architecture is presented, and the setup is used to perform some preliminary measurements. These first results indicate that some amount of multipath components can be recovered, even with limited angular resolution of a 4×4 beamsteering array.

Index Terms—mm-wave, 28 GHz, mapping, beamsteering

I. INTRODUCTION

The high bandwidths that are available at millimeter-wave (mm-wave) carrier frequencies offer the possibility of data rates much higher than at sub-6 GHz frequencies. The fifth generation (5G) new radio (NR) proposes the use of mm-wave frequencies going from 24.25 GHz to 52.6 GHz, with bandwidths between 100 and 400 MHz [1], [2]. To overcome the high path loss that occurs at mm-wave frequencies, antenna arrays with many antenna elements are envisioned, allowing for highly directional beamforming or beamsteering [1], [2].

While such systems allow for increased data rates, they also offer new possibilities in terms of localization and mapping. Knowledge of the direction of the mobile terminal (combined with the large bandwidths that allow for fine time resolution), localization of mobile terminals becomes a much easier task than with sub-6 GHz systems [3]. But the increase in bandwidth and size of the antenna arrays also allow for radar-like processing, allowing to map the environment surrounding the mm-wave transceivers [4].

While mm-wave systems share many similarities with radars, they also have some (important) differences. High-end radar systems often come with multiple RF chains and ADCs, allowing for multi-antenna processing in the digital baseband domain [5]. Current commercial off-the-shelf (COTS) 28 GHz transceiver often allow to do beamsteering digitally, but with only one single baseband signal [6], [7]. Moreover, radars send a well-known predefined waveform, which allows to simplify the processing at the radar receiver side [5]. In a 28 GHz system, the waveform sent by the transmitter will not be optimized for ranging and Doppler estimation, which will have to be done opportunistically [8]. Bistatic radars (where the Tx and Rx are not co-located) also require a local oscillator (LO) sharing mechanism, often through cables between the Tx and Rx [9]. This would be a major hindrance in 28 GHz systems, that would render the system unpractical.

In this paper, we propose a first investigation of environment mapping using a 28 GHz beamsteering system. In particular, the contributions are the following:

- we propose a hardware architecture, based on COTS elements, to allow for 28 GHz communications between a pair of transceivers;
- the system is used to try and identify multipath components (MPCs) between the pair of transceivers by steering the transceiver beam at both Tx and Rx side;
- an analysis of the MPCs that can and cannot be observed is provided, showing the limits of a beamsteering system for MPC identification.

While the analysis in this paper is still preliminary, it allows to highlight the importance and the limits of beamsteering systems (width of the main lobe, sidelobes, power of the line-of-sight) for environment mapping at 28 GHz.

II. CHALLENGES

There are multiple scientific and technical challenges for using 28 GHz transceivers for environment mapping. In the following, we assume 28 GHz transceivers

equipped with multi-antenna arrays that rely on beamsteering, i.e. the amplitude and phase shift of each antenna element can be controlled digitally, but there is only a single RF front-end and ADC, resulting in a single baseband signal (as opposed to multi-antenna arrays where the signal from each antenna is digitized and converted to a baseband signal). The challenges related to such arrays can be classified in three broad categories.

Multipath identification with beamsteering: Conventional multi-antenna arrays can rely on the baseband signal from each antenna to feed high-resolution algorithms (such as MUSIC, SAGE, etc.). In a beamsteering multi-antenna array, the beam can be pointed to all directions in space, but the beamwidth of the beam can hide smaller multipath components (MPCs) behind bigger ones (such as the Line-of-Sight (LoS) contribution). On top of large beamwidths, the presence of high sidelobes can also be problematic to identify MPC contributions. While high-resolution algorithms can be adapted for beamsteering arrays, they require careful calibration of the array for all possible amplitudes and phase shifts of the antenna elements. Moreover, steering the beam of the array in all directions can take up to several hundreds of milliseconds (or even seconds), making it harder to identify and track moving targets.

Compensating LO offset: A pair of 28 GHz transceivers can be used similarly to a bistatic radar. The transmitter and the receiver of a bistatic radar typically need to share a local oscillator (LO) to make radar processing possible. When sharing a LO is not possible, the LoS between the transmitter and the receiver is used to estimate the LO offset between Tx and Rx, as discussed below. However, it will take between a few milliseconds and several hundreds of milliseconds for the Tx and Rx to steer their beams into all (or some) directions of space. During this time, the LO offset will drift, which will affect the imaging or radar processing algorithms. Therefore, tracking the LO offset during the entire duration of the beamsteering will be necessary for efficient environment mapping.

Compensating the LoS component: When sharing a LO between Tx and Rx is impossible (such as in the case of satellite imaging), the LoS between the Tx and the Rx can be used to estimate the LO offset between transmitter and receiver. This requiring isolating the LoS component (in time and/or space), which for satellite-to-ground communications is relatively easy to achieve. In the case of 28 GHz femtocell communications, the LoS might be harder to isolate, especially when the beamwidth of the arrays is somewhat larger. High bandwidths (up to 400 MHz for 5G-FR2 systems) can help in isolating the LoS, but this will remain difficult for dense indoor environments. This will also be problematic for NLoS

environments, where new forms of processing will be required to extract the LO offset based on NLoS MPC contributions.

III. EXPERIMENTAL SETUP

We realize a pair of 28 GHz transceivers based on software-defined radios (SDRs). The transceiver architecture can be separated into three components: i) the baseband and intermediate frequency (IF) generation using SDRs, ii) the up- and down-conversion of IF signals to 28 GHz and iii) the beamsteering multi-antenna array at 28 GHz. A general block-diagram of the Tx is shown in Figure 1, the receiver has a very similar architecture.

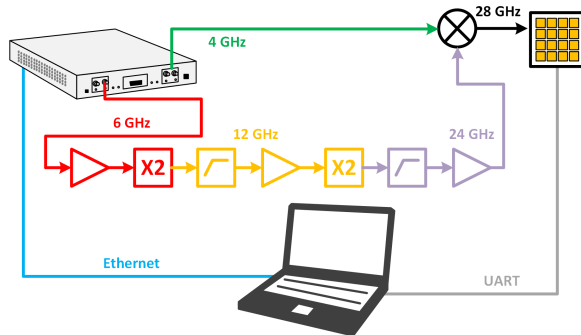


Fig. 1. Block-diagram of the 28 GHz transmitter.

Baseband and IF generation using SDRs: At the Tx side, we use USRP-X310 for generating a continuous 6 GHz pilot tone (that will be up-converted to 24 GHz), and we generate a baseband signal that is up-converted to 4 GHz IF (which will later be mixed with the 24 GHz signal to create a 28 GHz signal). In our setup, the transmitter sends data packets with random QPSK symbols with a bandwidth of 1 MHz. The packets are 1 ms long, and are sent periodically every 10 ms. At the Rx side, a USRP-X310 is also used for generating a continuous 6 GHz pilot tone (that will be up-converted to 24 GHz), while the 4 GHz signal (obtained by mixing the 28 GHz signal with the 24 GHz pilot tone) is further down-converted and digitized by the USRP-X310. The received data is stored on the host computer for further off-line processing. Both USRPs can be connected to a clock distribution system when we want to share the LO between both transceivers.

Up- and down-conversion of IF signals to 28 GHz: We use a fairly simple architecture to up- and down-convert the signals from 4 GHz to 28 GHz. First, we generate a 24 GHz pilot tone by up-converting a 6 GHz pilot tone to 24 GHz using two stages composed of frequency doublers, filters (to suppress undesired harmonics) and power amplifiers (to maximize the signal output). Since power amplifiers are active elements, an appropriate DC power generation architecture (not shown in Figure 1)

needs to be realized. At the Tx side, the 24 GHz pilot tone is then multiplied with the 4 GHz IF signal to create a 28 GHz signal. The receiver mixes the 28 GHz signal the 24 GHz pilot to obtain a 4 GHz IF signal. Note that there is no filtering after mixing to 28 GHz, since the antenna array will take care of filtering undesired harmonics.

28 GHz beamsteering antenna arrays: We use a COTS chipset for the 28 GHz antenna array, that is composed of a 4×4 rectangular antenna array. The amplitude and phase shift of each antenna element can be controlled digitally through an UART port. The resulting beam can be steered into a finite set of directions, i.e. 34 possible directions in the azimuth domain, and 34 possible directions in the elevation domain. Setting the beam of the antenna array currently takes about ten milliseconds, but this can be further optimized to reach 1 ms. The beam created by the 4×4 array has a half-power beamwidth between 15° and 25° (depending on the direction of steering), and sidelobes that are 8 to 20 dB below the main lobe (also depending on the direction of steering). In general the performances of the array degrade in the endfire directions, and are best in the broadside direction.

IV. MEASUREMENT RESULTS

A. Measurement scenarios

A first measurement campaign was held in an indoor office environment. While the measured scenarios are somewhat artificial, they allow to have first answers about the ability to identify multipath with 28 GHz beamsteering transceivers. In our experiments, the Tx and the Rx share a LO. The beams of the Tx and the Rx are swept over the horizontal plane such as to cover all possible pairs of Tx/Rx angles. Elevation is not considered in this paper, the beams are kept in the horizontal direction at all times.

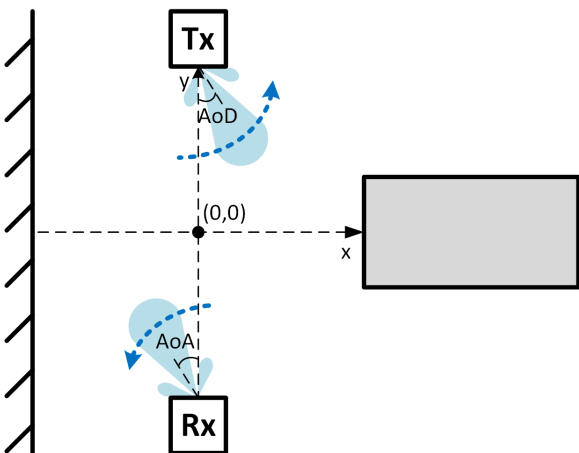


Fig. 2. Scenario of the measurements.

The measurement scenario is shown in Figure 2. The Tx and Rx are placed in an office with a brick wall on one side, and a metal closet on the other side. The Tx and Rx are facing each other, and are placed such that their x-coordinate is in the middle between the wall and the closet (which are separated 2.12 m apart). Several measurements, for different y-coordinates of the Tx and Rx, are taken and summarized in Table IV-A. In the first three measurements, Tx and Rx are at an equal distance of the line between the wall and the closet, such that there should be a first order-reflection (corresponding to Snell's law) on the wall and on the closet at a Tx/Rx angle of 30° , 45° and 60° , respectively. In the fourth and fifth measurements, the reflection on the closet can only happen through diffraction (the wall will still have a reflection according to Snell's law at a Tx/Rx angle of 41°). It is important to note that the measurement equipment was placed and oriented as accurately as possible, but that small orientation errors (typically between -5° and $+5^\circ$) are inevitable.

TABLE I
TX/RX X- AND Y-COORDINATE (IN M) OF THE DIFFERENT MEASUREMENTS.

Meas.	Tx-x	Tx-y	Rx-x	Rx-y
1	0	1.84	0	-1.84
2	0	1.06	0	-1.06
3	0	0.61	0	-0.61
4	0	1.84	0	-0.61
5	0	0.61	0	-1.84

B. Data post-processing

During the experiments, the Tx beam is kept in a fixed direction while the Rx beam sweeps all possible angles, after which the Tx beam is moved and the whole process is repeated. For each pair of Tx/Rx beam directions, 0.5 s of data is recorded, corresponding to 50 data packets. In a post-processing stage, the data packets are extracted by applying a correlation function, and the mean power of each packet is calculated. Finally, the power of the 50 data packets (corresponding to a single Tx/Rx beam direction) is averaged.

C. Mapping results

We first provide a pure LoS measurement with the Tx and Rx at a short distance (1.50 m), without any reflections in the near vicinity. The power as a function of the transmit direction (Angle-of-departure or AoD) and receive direction (Angle-of-arrival or AoA) is shown in Figure 3. The beamwidth of the Tx and Rx array can clearly be observed, as can be the sidelobes that are about 10 dB below the main lobe. It is already clear from this figure that MPCs close to the LoS direction will be hard to distinguish, and that even sidelobes will be able to hide smaller MPCs.

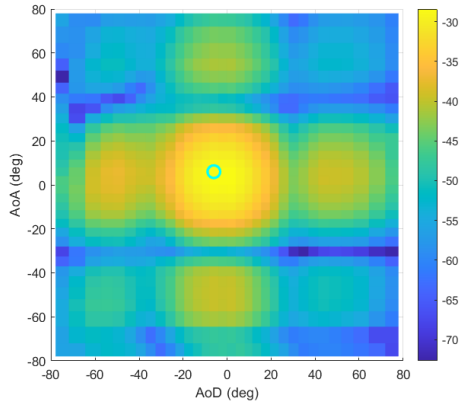


Fig. 3. AoA/AoD map for a LoS scenario without reflections. The cyan dot represents the LoS direction.

In the case of measurement 1 shown in Figure 4, the reflection on the wall and on the closet can be observed from the AoA/AoD map. It should be noted that while the reflection corresponding to Snell's angle (indicated by a cross) can be identified, diffractions along the wall or along the closet's edges cannot be identified. It should also be noted that the power corresponding the MPCs is similar to the power of the sidelobes corresponding to the LoS, and that careful processing will be necessary to ascertain the contributions of MPCs.

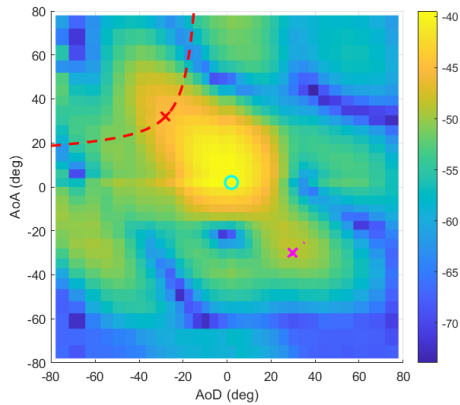


Fig. 4. AoA/AoD map for measurement 1 (Tx and Rx are separated by 3.68 m). The cyan dot represents the LoS direction, the red line represents the wall and the magenta line represent the closet.

The conclusions for the second measurement (shown in Figure 5) are relatively similar. The contributions of the wall and closet reflections can still clearly be identified.

For the third measurement, the contributions from the wall and closet reflections can no longer be identified. In this case, the power of the reflected MPCs is too low with respect to the power of the LoS component. This

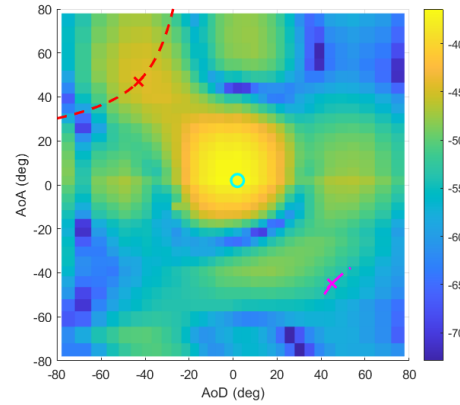


Fig. 5. AoA/AoD map for measurement 2 (Tx and Rx are separated by 2.12 m). The cyan dot represents the LoS direction, the red line represents the wall and the magenta line represent the closet.

is a typical situation where the LoS component “blinds” the other direction. This could possibly be resolved using high-resolution algorithms, but a careful calibration of both transmit and receive arrays (for all possible beam direction) is required for such algorithms.

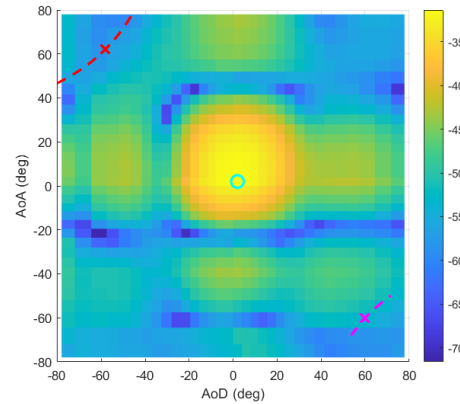


Fig. 6. AoA/AoD map for measurement 3 (Tx and Rx are separated by 1.22 m). The cyan dot represents the LoS direction, the red line represents the wall and the magenta line represent the closet.

Figures 7 and 8 show the AoD/AoA map for measurements 4 and 5. The conclusions are roughly similar as before for the wall reflection, i.e. the wall reflection can be identified, although it is partially blinded by the LoS component. The reflection on the cabinet (which does not correspond to Snell's law, but rather to a diffraction) cannot clearly be seen in those measurements. A high-resolution algorithm might be able to identify a contribution, but simple beamsteering does not have sufficient resolution to detect the diffracted MPCs.

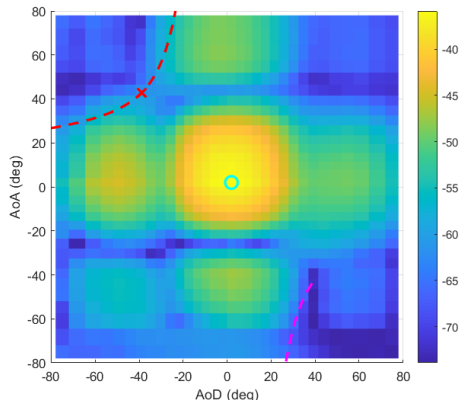


Fig. 7. AoA/AoD map for measurement 4 (Tx and Rx are separated by 2.45 m, but not equidistantly w.r.t the closet). The cyan dot represents the LoS direction, the red line represents the wall and the magenta line represent the closet.

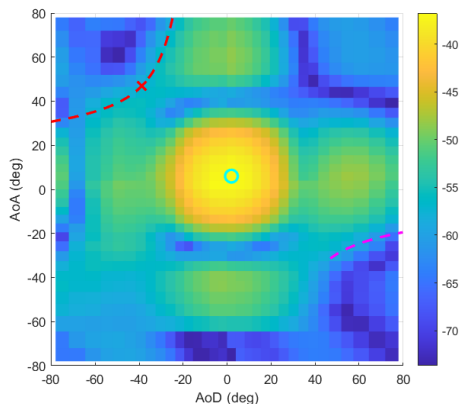


Fig. 8. AoA/AoD map for measurement 5 (Tx and Rx are separated by 2.45 m, but not equidistantly w.r.t the closet). The cyan dot represents the LoS direction, the red line represents the wall and the magenta line represent the closet.

V. CONCLUSION AND FUTURE WORK

In this paper, we performed a preliminary analysis of environment mapping using 28 GHz beamsteering transceivers. A SDR-based transceiver architecture, using 4×4 arrays, was presented. A preliminary measurement campaign was performed in an indoor environment, to identify whether the power of simple reflections could be identified using beamsteering at the transmitter and at the receiver. The measurement result show a somewhat mitigated picture: the MPC contribution can be identified if the power of the MPC is not too low with respect to the LoS, such that it is not hidden by the LoS sidelobes or the LoS itself. Reflections following Snell's law can for the most part be identified, whereas diffracted rays appear less clearly on an AoD/AoA map. Our future work will focus on using high-resolution algorithms

(such as expectation-maximization algorithms) to identify MPC contributions. This will, however, require a careful calibration of the transmitter and the receiver system. Adding the delay domain in the imaging (using high-bandwidth systems) should also allow to further identify the MPC contributions. The next step will then be to move to an over-the-air synchronization system, where the Tx and Rx transceivers do not share a common, cable-connected LO. Similarly to bistatic imaging in satellite systems, we will rely on the LoS to calibrate the receiver LO. However, since the process of mapping with beamsteering is not instantaneous, we will need to continuously track the LO offset to compensate for it appropriately. Finally, we will consider NLoS scenarios, where LO offset compensation needs to be done relying on MPCs, rather than on the LoS component.

ACKNOWLEDGMENT

The authors acknowledge the financial support of the Belgian F.R.S.-F.N.R.S. through the MIS project F.4538.22 "SYNCH-NET".

REFERENCES

- [1] Xingqin Lin, Jingya Li, Robert Baldemair, Jung-Fu Thomas Cheng, Stefan Parkvall, Daniel Chen Larsson, Havish Koorapaty, Mattias Frenne, Sorour Falahati, Asbjorn Grovlen, and Karl Werner, "5g new radio: Unveiling the essentials of the next generation wireless access technology," *IEEE Communications Standards Magazine*, vol. 3, no. 3, pp. 30–37, 2019.
- [2] Eric Mercier, "Beyond 5g amp; technologies: A cross-domain vision," in *2020 IEEE Symposium on VLSI Technology*, 2020, pp. 1–2.
- [3] Ojas Kanhere, Sanjay Goyal, Mihaela Beluri, and Theodore S. Rappaport, "Target localization using bistatic and multistatic radar with 5g nr waveform," in *2021 IEEE 93rd Vehicular Technology Conference (VTC2021-Spring)*, 2021, pp. 1–7.
- [4] Purushottama Lingadevaru, Bethi Pardhasaradhi, Pathipati Srihari, and GVK Sharma, "Analysis of 5g new radio waveform as an illuminator of opportunity for passive bistatic radar," in *2021 National Conference on Communications (NCC)*, 2021, pp. 1–6.
- [5] "Imaging radar using cascaded mmwave sensorreference design," Tidedp-01012, Texas Instruments, 2019.
- [6] Michael D. Foegelle, "New and continuing measurement challenges for 5g mmwave and beamforming technologies," in *2019 13th European Conference on Antennas and Propagation (EuCAP)*, 2019, pp. 1–5.
- [7] Wei Fan, Pekka Kyosti, Moray Rumney, Xiaoming Chen, and Gert Frolund Pedersen, "Over-the-air radiated testing of millimeter-wave beam-steerable devices in a cost-effective measurement setup," *IEEE Communications Magazine*, vol. 56, no. 7, pp. 64–71, 2018.
- [8] Laurent Storrer, Hasan Can Yildirim, Morgane Crauwels, Evert I. Pocoma Copa, Sofie Pollin, Jerome Louveaux, Philippe De Doncker, and Francois Horlin, "Indoor tracking of multiple individuals with an 802.11ax wi-fi-based multi-antenna passive radar," *IEEE Sensors Journal*, vol. 21, no. 18, pp. 20462–20474, 2021.
- [9] Laurent Storrer, Hasan Can Yildirim, Claude Desset, Marc Bauduin, Andre Bourdoux, and Francois Horlin, "Clutter removal for wi-fi-based passive bistatic radar," in *2020 IEEE 91st Vehicular Technology Conference (VTC2020-Spring)*, 2020, pp. 1–5.